ACS APPLIED MATERIALS & INTERFACES

www.acsami.org

Research Article

Self-Powered Smart Arm Training Band Sensor Based on Extremely Stretchable Hydrogel Conductors

Feifan Sheng, Jia Yi, Shen Shen, Renwei Cheng, Chuan Ning, Liyun Ma, Xiao Peng, Wen Deng, Kai Dong,* and Zhong Lin Wang*

Cite This: https://doi.org/10.1021/acsami.1c12378

Read Online

ACCESS | Metrics & More | Article Recommendations | Supporting Information

ABSTRACT: The development of elastic electronic technology has promoted the application of triboelectric nanogenerators (TENGs) in flexible wearable electronics. However, most of the flexible electronics cannot achieve the requirements of being extremely stretchable, transparent, and highly conductive at the same time. Herein, we report a TENG constructed using a double-network polymer ionic conductor sodium alginate/zinc sulfate/poly acrylic-acrylamide (SA−Zn) hydrogel, which exhibited outstanding stretchability (>10,000%), high transparency (>95%), and good conductivity (0.34 $S \cdot m^{-1}$). The SA−Zn hydrogel TENG (SH-TENG) could harvest energy from typical human movements, such as bending, stretching, and twisting, which could light up 234 green commercial LEDs easily. Additionally, the SH-TENG can be used to prepare a self-powered smart training band sensor for monitoring arm stretching motion. This work may provide an innovative platform for accessing the next generation of sustainable wearable and sports monitoring electronics.

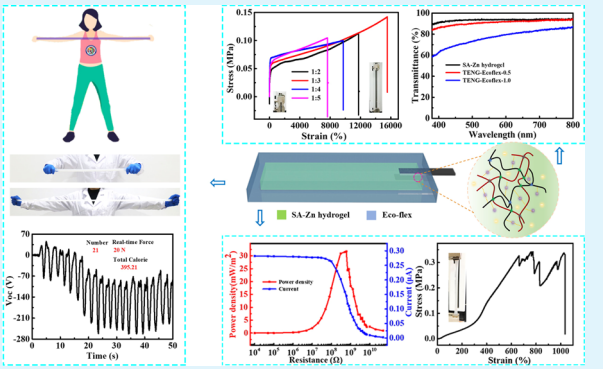

KEYWORDS: *hydrogel, stretchability, conductivity, triboelectric nanogenerator, self-powered sensor*

1. INTRODUCTION

Flexible electronics have sparked extensive attentions for their widespread applications, such as smart skins, energy harvesters, wearable electronics, and health monitors.[1−5] These devices should have the ability of bending, folding, twisting, and stretching, while maintaining the original electronic and structural properties. Simultaneously, flexible electronics are also moving toward lightweight,[6] miniaturization,[7,8] environmental friendliness,[9] flexibility,[8,10] stretchability,[11,12] and intelligence.[13,14] Aiming to realize fully flexible electronics, suitable flexible power supply equipment[15−17] and a portable energy solution are required.[18,19] Triboelectric nanogenerators (TENGs),[20−22] which can harvest energy from surrounding mechanical movements,[23−26] have attracted great attentions due to their environmental friendliness, cost-effectiveness, universal applicability, and high energy conversion efficiency at low frequencies.[27−31] Recently, numerous researchers have devoted their efforts to fabricate stretchable TENGs and expand their potential applications.[12,32,33] These TENGs can collect energy which is generated by human movements, such as walking, running, swinging, or tapping.[34,35] However, the development of flexible and stretchable TENGs is challenging due to the lack of the high-performance elastic electrodes. Therefore, huge attentions are being focused on ultra-stretchable conductive electrodes to achieve various extreme deformations and good conductivity.[36]

For stretchable electrode materials, there are mainly three manufacturing methods: one is rigid conductive material after geometric structural design, the other is conductive material mixed with an elastomer, and the last is material with essentially high elongation and conduction.[37,38] However, for rigid conductive materials, the design of a tensile structure is always complex without significant improvement in tensile performance.[14,39] For the second kind of materials, conductive fillers such as carbon nanotubes,[40] graphite spray,[41] liquid metals,[42] silver nanowires,[43,44] and conductive polymers[45] have been embedded into extendible matrixes, which significantly improve the conductivity of the elastomers. However, most current conductors possess a poor electromechanical performance and adhesion of fillers on elastomers due to an uneven mixing, thus leading to an insufficient compatibility between conductive fillers and adjacent elastic networks.[46] Although the abovementioned soft conductors can work effectively under moderate stretching or deformation, these materials are limited

Received: July 1, 2021

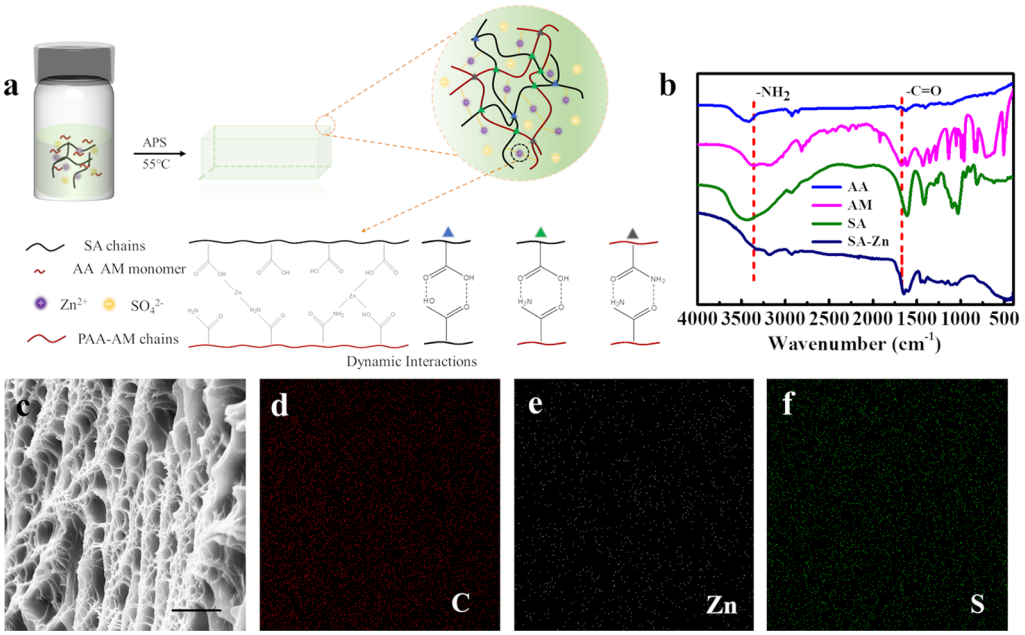

Figure 1. Characterization of the SA−Zn hydrogel. (a) The preparation process and the reaction principle of the SA−Zn hydrogel. (b) The chemical structure of FTIR spectra of the AA, AM, SA and SA−Zn. (c,d−f) SEM image and EDS mapping of SA−Zn sample with a scale bar of 10 μm.

in terms of large elongation, transparency, and high electrical conductivity at the same time.

Unlike the conductive composite materials described above, stretchable and conductive hydrogel electrolyte is particularly attractive. Hydrogel has become a promising material in imitating biological systems. Salt-containing hydrogel is an ionic conductor, which has the advantages of easy manufacturing, low cost, high elongation, and high conductivity.[31] It not only can absorb and store a certain amount of water through chemical or physical cross-linking but also has liquid-like rapid diffusion properties and solid-like mechanical properties,[47] enabling it with high flexibility, elasticity, and water content similar to biological tissue.[48] In addition, researchers have built different dynamic cross-linked networks, endowing these soft-ion hydrogels with practical functions, such as stretchability, conductivity, biocompatibility, and so on. It is worth noting that the electrical resistance of an ionic conductor hydrogel will gradually increase as it stretches. In addition, the change in resistivity of hydrogels with strain is much smaller than that of electronic conductors.[49] Through the combination of electronic properties and mechanical properties, the field of ionotronics of hydrogels was established, including physical and chemical sensors, power generation, and storage devices.[50,51] However, most of the hydrogels reported cannot meet the requirements of ultrastretchability, transparency, and high conductivity at the same time.[52−54] Therefore, it is necessary to design hydrogels that can tackle these bottlenecks simultaneously, which hence can be used as electrodes for flexible electronics.[55−57]

Therefore, we introduced an ultrastretchable TENG based on a tensile ionic conductor hydrogel, which can collect human movement energy and perform real-time motion monitoring. The hydrogel was synthesized with zinc (Zn) in polymer strategy with sodium alginate (SA) and poly(acrylic-acrylamide) (PAA). A double-network structure hydrogel (SA−Zn hydrogel) was constructed using SA and PAA, and there is a dynamic reversible interaction between the metal ion and the double-network structure. High conductivity was achieved by ionic transportation through polymer chains. The SA−Zn hydrogel showed high transparency, super stretchability, excellent conductivity, which could also recover to its original state after being stretched for a period of time. In addition, SA−Zn hydrogel could be used as TENGs by simply encapsulating with silicone rubber elastomers. The SA−Zn hydrogel TENG (SH-TENG) exhibited good electrical output performance even under high-tensile states. This device with high sensitivity and good stability provides a broad promising possibility for the development and applications in super-stretchable self-powered sensors, wearable power sources, and health and exercise monitoring platforms.

2. RESULTS AND DISCUSSION

2.1. Synthesis and Characterization of SA−Zn Hydrogel. In this work, SA, AA, and AM monomers and zinc sulfate ($ZnSO_4$) were chosen to prepare a super elongated ionic conductor hydrogel electrode. The double-network structure and dynamic interaction constructed using the two macromers (SA and PAA) greatly improve the tensile properties of the hydrogel. In addition, it can recover to the original shape within a period of time after over-stretching. Moreover, Zn ions can be combined with the double-network structure on the polymer chain to control ion migration, which can improve the conductivity and stretchability of the hydrogel. As shown in Figure 1a, the dynamic cross-linking process of SA, AA, and AM monomers forms a double-network hydrogel.

The prepared hydrogel freeze-dried samples were characterized by FTIR for their characteristic peaks. As depicted in Figure 1b, characteristic peaks of AA at 3430, 1722, and 1620 cm^{-1} belong to stretching vibration of −OH, −C═O, and −C═C, respectively. The absorption peaks at 1670, 3174, and 3340 cm^{-1} are the −C═O, −C═C, and $-NH_2$ stretching vibration of AM, respectively. The peaks at 3450, 2929, 1610, and 1180 cm^{-1} are the −OH, $-CH_3$, −C═O, and −C−O−C− stretching vibrations of SA, respectively. All the absorption

https://doi.org/10.1021/acsami.1c12378
ACS Appl. Mater. Interfaces XXXX, XXX, XXX−XXX

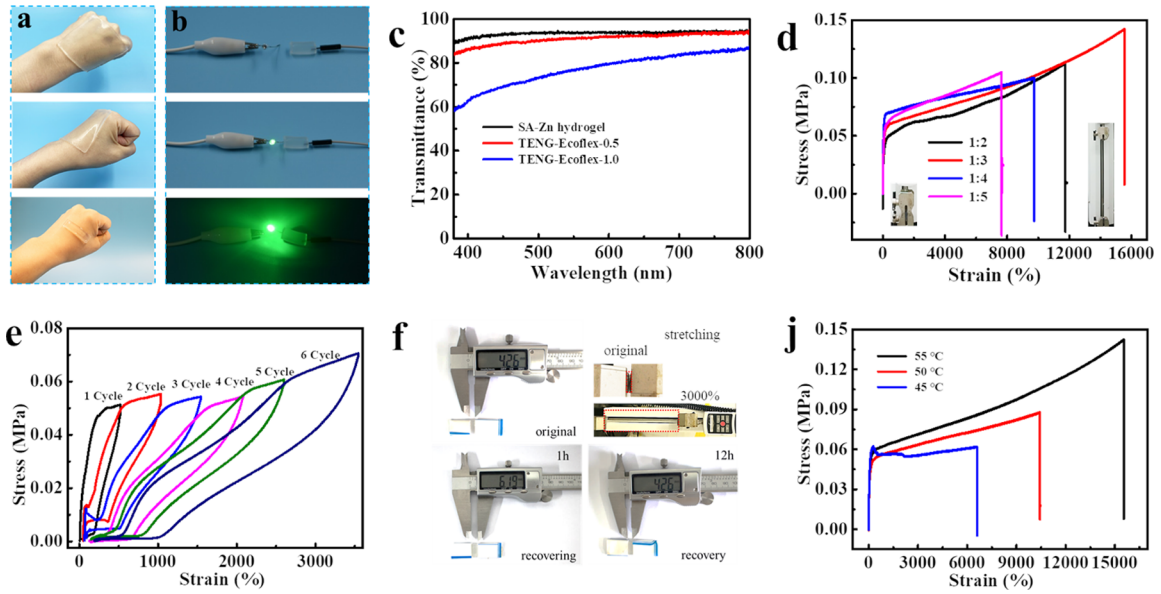

Figure 2. Mechanical performances of the SA−Zn hydrogel. (a,b) Photographs showing the compliance, transparency and conductivity of SA−Zn hydrogel. (c) Ultraviolet−visible transmittance spectra of the SA−Zn hydrogel and SH-TENG with different thickness encapsulation of ecoflex (0.5 and 1.0 mm). (d) Tensile curves of different proportions of AA and AM of mechanical properties for hydrogels. Inter is the images of original and stretched state of the SA−Zn hydrogel with AA and AM feed ratio of 1:3. (e) Loading-unloading tensile curves of SA−Zn hydrogel at 500-3500% strains. (f) Reversible stretching of the SA−Zn hydrogel (j) Tensile curves of different temperature of mechanical properties for the SA−Zn hydrogel. Unless otherwise specified, all stretching rates are fixed at 50 mm min^{-1}.

peaks of SA−Zn hydrogel in the FTIR spectrum are confirmed by the presence of all the groups. AA, AM, and SA peaks at 3328, 2925, 1650, 1612, and 1135 cm^{-1} corresponding to the stretching vibrations were observed, demonstrating that all the characteristic groups are successfully formed in the polymer network of SA−Zn hydrogel.

Furthermore, the SEM image of SA−Zn hydrogel was captured. Figure 1c shows that the freeze-dried SA−Zn hydrogel exhibits an obviously typical three-dimensional network microstructure with regularly distributed large pores. Figure 1d−f are the EDS mapping images of C, Zn, and S elements, respectively. The above results demonstrate that Zn^{2+} and SO_4^{2-} ions are uniformly distributed and incorporated in the SA−Zn hydrogel.

2.2. Mechanical Properties of SA−Zn Hydrogel. As shown in Figure 2a, the images of the prepared hydrogel were obtained by optimizing different feed ratios of different reaction monomers and reaction conditions. When SA−Zn hydrogel was used as a conductor, by connecting with a green LED to form a complete circuit, the LED could be lighted by connecting an external 9 V power supply (Figure 2b). Based on the optimal feed ratios, the synthesized SA−Zn hydrogel with a thickness of 2.0 mm has a good transparency in the visible light region, and the average transmittance is more than 95% (Figure 2c). The corresponding SA−Zn TENG with thicknesses of 0.5 and 1 mm was encapsulated with ecoflex, which shows a transmittance of 94 and 87%, respectively. This makes it possible to manufacture more transparent flexible displays and develop integrated visual interactive wearable devices.

The mechanical property of ion-conducting hydrogel is the most important factor for its application as a stretchable TENG sensor. Thus, the mechanical properties with different ratios of AA and AM were compared. As the AM content rises, the SA−Zn hydrogel shows a notable increase in breaking strain and tensile strength, followed by a remarkable decrease (Figure 2d). This abnormal phenomenon is likely to be caused by the increased cross-linking site density and dynamic equilibrium of zinc ions with the two polymer chains.[58,59] The SA−Zn hydrogel can obtain an astonishingly high tensile strain of more than 10,000% at a high strength of 0.15 MPa with an optimal AA and AM feed ratio of 1:3. It demonstrates that SA−Zn hydrogel has an outstanding stretchability, which is much higher than that of most conductive hydrogels. To further prove the super-stretchability of the prepared hydrogel, the hydrogel with an initial length of 2.0 mm was stretched over 20 cm without breaking (Movie S1, Supporting Information). The excellent super-stretchability of SA−Zn hydrogel is due to the dynamic coordination between Zn^{2+} ions and the molecular chains in the double network and at the same time, a part of the electrostatic mutual attraction with it.

Figure 2e displays the stretching and releasing process under different tensile strains ranging from 500 to 3500% at 50 mm·min^{-1}. It shows a quantitative evaluation of the self-recovery characteristic of the prepared hydrogel. When the stretching is lower than 1000%, the tensile curve of SA−Zn hydrogel shows a small hysteresis loop and then recovers to its original state quickly, which verifies that the prepared hydrogel has excellent self-recovery performance after low elongation. The stretching curve of SA−Zn hydrogel indicates that the stretching and releasing process has obvious hysteresis as the tensile strain exceeds 1000%. After removing the tensile force, the prepared hydrogel cannot immediately return to its original state. The reconstruction speed of the dynamic interactions of the internal molecules of the hydrogel cannot meet the reconstruction speed of the double-network framework structure, which leads to the hysteresis of the shape of the tensile release curve. However, as long as there is enough time, the SA−Zn hydrogel can be restored to its original state.

As shown in Figure 2f, after the SA−Zn hydrogel is being stretched to 3000%, it can be restored to about 50% of its original state within 1 h and can be completely restored to its

https://doi.org/10.1021/acsami.1c12378
ACS Appl. Mater. Interfaces XXXX, XXX, XXX−XXX

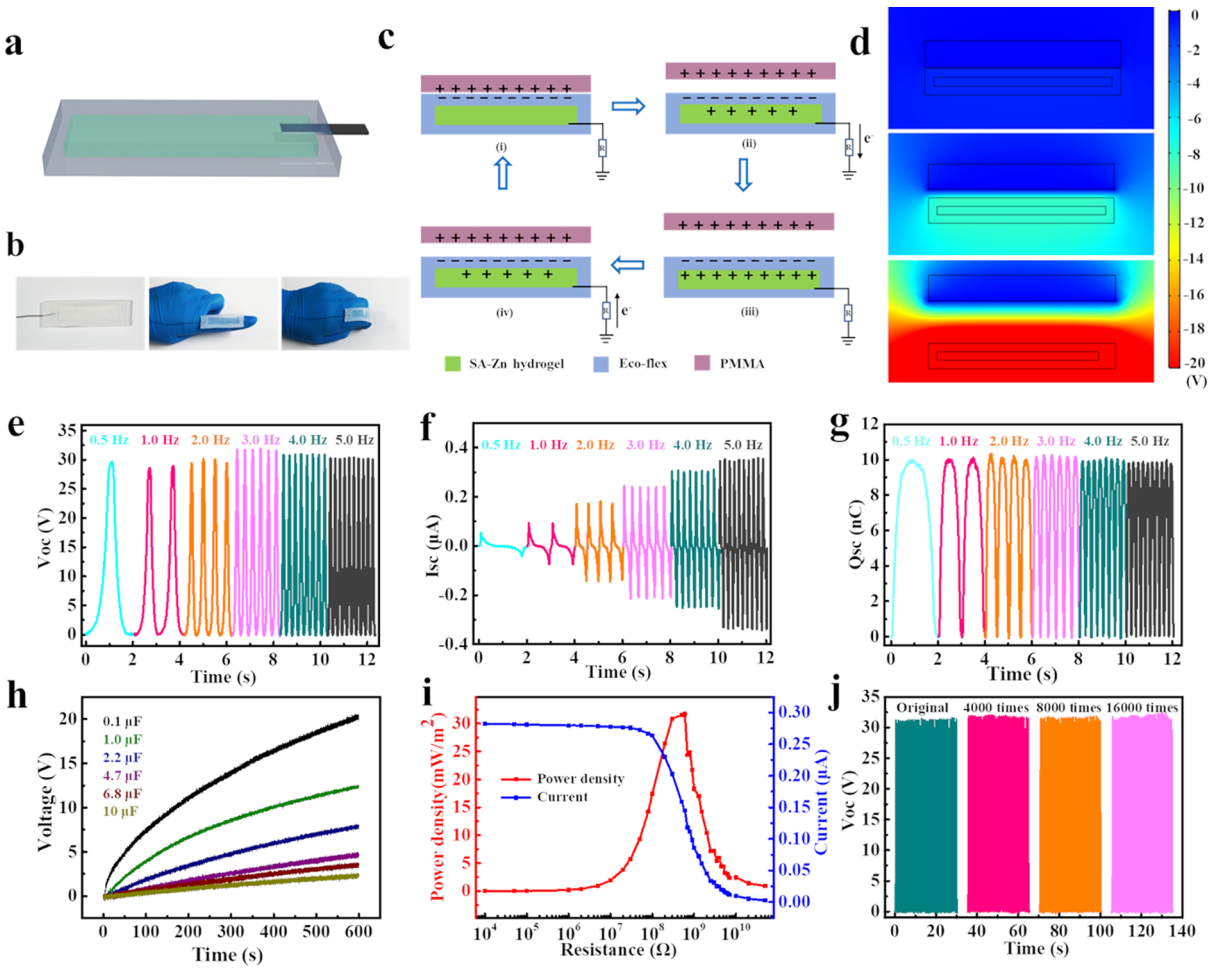

Figure 3. Performance of nanogenerator based on SA−Zn hydrogel. (a) Schematic diagram of the SA−Zn hydrogel TENG. (b) The photographs of the SH-TENG in its original and foldable state. (c) The energy harvesting mechanism of the SH-TENG. (d) Simulation schematics of SH-TENG. (e) V_{OC}, (f) I_{SC}, and (g) Q_{SC} of SH-TENG under different working frequency (0.5−5 Hz) with force load at 3 N. (h) The charging voltage curves of different commercial capacitors (0.1, 1.0, 2.2, 4.7, 6.8, and 10 μF) by the SH-TENG. (i) The relationship between current and power density and external load resistance with an external load resistance from 10^4 to 5×10^{10} Ω (at 3 Hz). (j) V_{OC} of TENG that continuously operation for ∼16,000 cycles (at 1 Hz).

original state within 12 h. The self-recovery to the initial state is due to the dynamic interactions of molecules in the double-network structure and the movement of molecular chains in hydrogel. When the hydrogel is in a released state, the stretched molecular chains will gradually shrink and wind freely. When the separated molecular chains come in contact with Zn(II) again, the broken molecules are easily reconnected under dynamic interactions. Then, SA−Zn hydrogel dynamic molecular interactions are continuously connected and recombined to rebuild the double-network framework until it recovers to its original state.[60] In addition, the SA network with physical cross-linking has dynamic energy dissipation that can improve the tensile recovery of SA−Zn hydrogels, while the PAA network produced by chemical cross-linking can enhance the mechanical strength property of SA−Zn hydrogel.[48]

Similarly, the temperature in the process of synthesizing the hydrogel is another important factor that affects the mechanical properties of the prepared hydrogels. The effects of different reaction temperatures (such as 45, 50, 55, and 60 °C) on the tensile performance of the SA−Zn hydrogel are compared (Figure 2j). With the increasing temperature, the mechanical properties enhance sharply. When the temperature reaches 55 °C, the hydrogel has the best mechanical properties. When the reaction temperature exceeds 55 °C, the overall performance of the synthesized hydrogel will drop sharply. The intrinsic viscosity and mechanical properties of the copolymer suddenly decrease with the increase in the reaction temperature to a certain point, which is in line with the kinetic law of free radical polymerization. In the free radical reaction, the relationship between the total polymerization rate constant (K) and temperature (T) obeys the Arrhenius equation[61]

$$K = Ae^{-E/RT} \tag{1}$$

From formula (1), it can be seen that the polymerization rate, self-crosslinking degree, and product conversion rate are small at low temperature, which increases the soluble part of the resulting product. In addition, the grafted polymer cannot form an effective three-dimensional network structure copolymer. The final polymer has a small molecular weight, which brings about a poor mechanical property. Upon further increasing the reaction temperature, the reaction process of free radicals evidently promotes. Besides, the increase in the reaction temperature can facilitate the reaction of the chain transfer and termination, thereby increasing the content of the oligomer and decreasing the mechanical properties of products.[62] Therefore, the optimum reaction temperature is

https://doi.org/10.1021/acsami.1c12378
ACS Appl. Mater. Interfaces XXXX, XXX, XXX−XXX

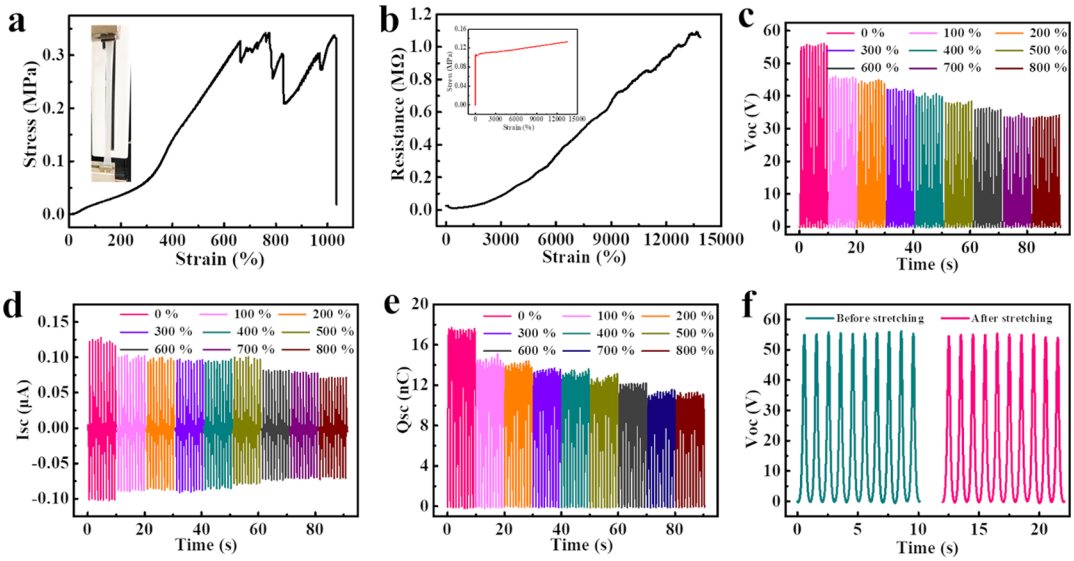

Figure 4. Physical properties of SH-TENG under tension. (a) Tensile curve of SH-TENG. Insert is the SH-TENG at stretched state (700% strain). (b) Real-time resistance change resistance variation of SA−Zn hydrogel under different tensile strains. Insert photograph is the real-time tensile stress−strain curve. (c) V_{OC}, (d) I_{SC}, and (e) Q_{SC} of SH-TENG at different strain levels. (f) The stability of SH-TENG under tensile strain.

55 °C (Figure 2j). All the results indicate that the mechanical properties of the prepared hydrogel can be adjusted over a wide range, enabling more selectivity and higher adjustability when applied to e-skin sensing elements or extendible electronics.

2.3. Electrical Output Performance of the SH-TENG. The hydrogel is used as an ionic conductor electrode, and the encapsulation layer is integrated to construct a transparent and stretchable SH-TENG (Figure 3a). In order to create a space for storing and sealing the hydrogel electrode, a layer of hydrogel is first attached to an elastomer silicone rubber substrate (ecoflex-0010) and a thin copper wire is inserted into the hydrogel as a conducting wire. Then, silicone rubber encapsulates the hydrogel to form a sealed sandwich structure (Figure 3b), which can prevent the SA−Zn hydrogel from drying out quickly.

Figure 3c demonstrates the operating mechanism of the SH-TENG. Once the PMMA (or other dielectric material not silicone rubber) moves into contact with the silicone rubber layer, a positive charge generates at the interface. Silicone rubber produces an opposite polarity and the same amount of negative charges as PMMA. At this time, see from Figure 3c (i), due to a complete balance between the frictional charges, no electrons flow in the external circuit. When PMMA and ecoflex separate and move upward, the conductive hydrogel produces a positive charge to compensate for the negative charge on the surface of ecoflex. In the above process, electrons flow from the SA−Zn hydrogel to the copper wire, generating a measurable but instantaneous current signal (Figure 3c, from (i) to (ii)). When PMMA moves down and approaches ecoflex, the entire process is reversed (Figure 3c (ii)). As shown in Figure 3c, from (iii) to (iv), the positive charges induced in the copper wire decrease, leading to the electrons flowing in the opposite direction. The SH-TENG continuously generates alternating current by repeating the periodic operation.

The potential distribution of the SH-TENG under the periodic state of contact and separation state between PMMA and silicone rubber was simulated using COMSOL software (Figure 3d). The electrical output performance of the SH-TENG under various frequencies was measured under a force load of 3 N (Figure 3e−g). When the contact area is 4 × 1 cm^2, it is found that the open-circuit voltage (V_{OC}) and short-circuit charge transfer (Q_{SC}) remain relatively stable and reach 30 V and 10 nC, respectively. As the periodic frequency continues to increase, the short-circuit current (I_{SC}) increases from small to 0.5 μA. Under the action of a linear motor, Figure 3h shows the SH-TENG charging different capacitors at a frequency of 1 Hz with a rectifier bridge. The maximum value of the charging voltage increases with the decrease in capacitance.

For different application scenarios, the SH-TENG can drive loads under different resistances. The I_{SC} and power density in series with various external resistors (10^4 to 5 × 10^{10} Ω) are studied, and the effective output power of the SH-TENG can be evaluated. Figure 3i indicates that the current in the SH-TENG declines with increasing external resistance. The power density can reach a maximum of 32 $mW{\cdot}m^{-2}$ at an external resistance of 0.6 GΩ. The applied frequency, external load, and contact area are 3 Hz, 3 N, and 4 × 1 cm^2, respectively. As shown in Figure 3j, it demonstrates the output voltage stability of the SH-TENG under 16,000 contact separation continuous loading cycles. It can be found that the voltage does not drop significantly, which clearly illustrates that the SH-TENG has a remarkable durability and practical application value. The SH-TENG can also keep its original output performance without significant degradation when the hydrogel is packaged with ecoflex for 20 days. This clearly shows that the SH-TENG prepared after direct encapsulation of the hydrogel has excellent stability (Figure S17).

As shown in Figure 4a, the mechanical properties of the SH-TENG encapsulated with silicone rubber (ecoflex 00-10) was studied through the stress−strain curve. The fracture strain of the SH-TENG is about 1035%, and the fracture stress is about 0.35 MPa, which is twice more than that of the hydrogel stress. When the breaking strain of the SH-TENG is about 780%, small damages appear in the device, and large damages occur

https://doi.org/10.1021/acsami.1c12378
ACS Appl. Mater. Interfaces XXXX, XXX, XXX−XXX

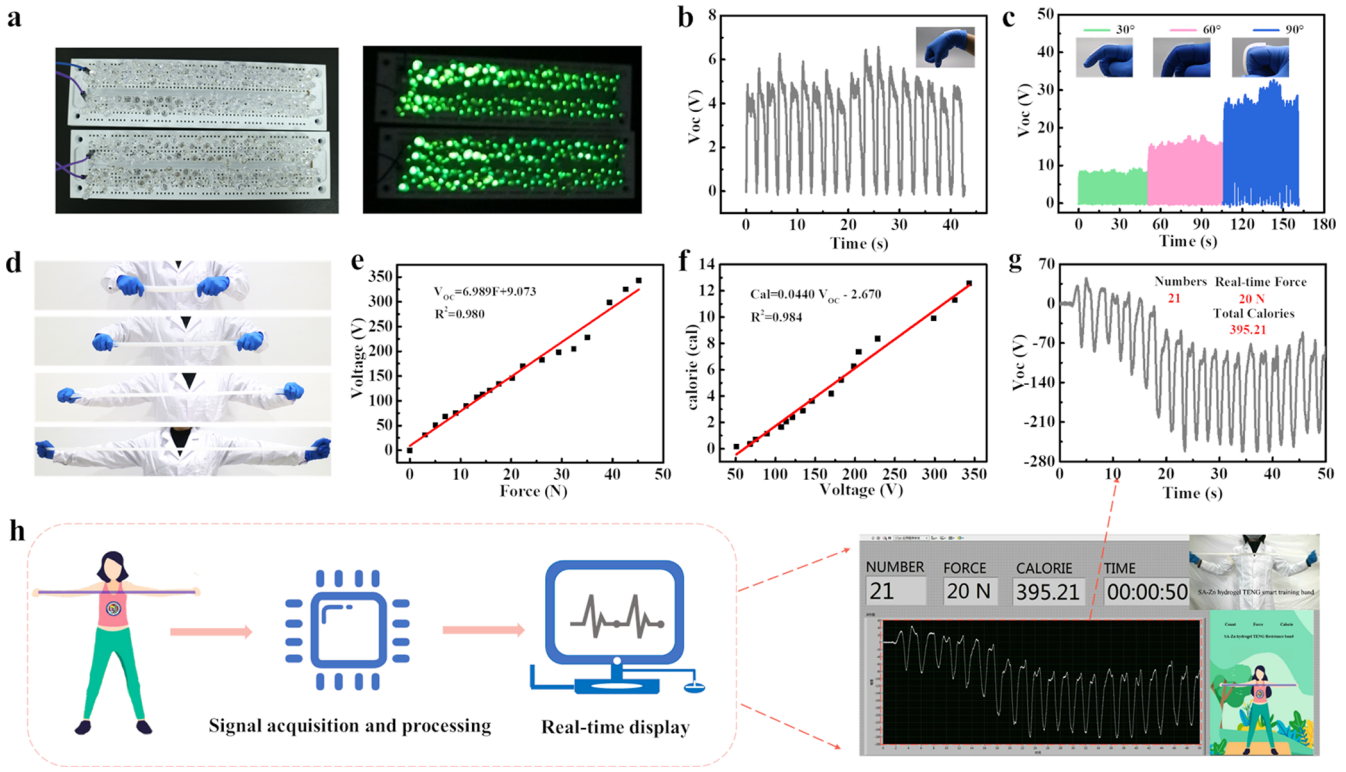

Figure 5. Application demonstration of SH-TENG. (a) Photograph showing that the TENG can lighting 234 commercial green LEDs. (b) Output signal of SH-TENG under motion state of wrist. Inset is the SH-TENG attached on the wrist. (c) The voltage outputs of the SH-TENG under 30, 60, and 90° bending angles of the finger. The insets are pictures of the SH-TENGs fixed on the fingers. (d) Photographs of different stretching states of the SH-TENG. (e) The relationship between force and output voltage by stretching the SH-TENG. (f) Calories consumed during stretching of SH-TENG. (g) Application of the SA−Zn-TENG smart training band. (h) Real-time demonstration process in the actual application of the self-power smart elastic belt system, including a signal acquisition and processing system, and a real-time software output interface.

above 830%. Therefore, the maximum tensile force in the experiment is limited at 800%.

In addition, the output stability during the stretching process of the hydrogel-based TENG is also significant. It is necessary to investigate the real-time resistance change of the SA−Zn hydrogel under applied tensile strain. As shown in Figure 4b, when the hydrogel reaches its maximum tensile strength, the resistance of the hydrogel is about 1.0 MΩ. When the elongation of the SH-TENG is lower than 1000% (Figure 4a), the change in resistance and conductivity of the hydrogel can be ignored, enabling a wide workable strain range of the conductor. Furthermore, it can also be verified in the Movie S2 (Supporting Information) that the light of the LED is not extinguished, which is consistent with the former demonstration.

The power generation capacity of the TENG under extreme tensile conditions was tested, and its planar direction was evaluated under different tensile strain conditions. The TENG can still collect energy and drive the load when it is greatly stretched in the long axis direction. The output of V_{OC}, I_{SC}, and Q_{SC} of the SH-TENG in different tensile strain states with the same external impact force is shown in Figure 4c−e, respectively. The electrical output decreases with the increase in the stretching length, which may be attributed to the change in the resistance of the conductor hydrogel during the stretching process and the narrower contact area with ecoflex. The deformation and electricity generation process for the stretching deformation is explored also. Figure S14 shows that the electrical output of the SH-TENG increases with the increase in the stretching length, which may be attributed to the decrease in the gap between hydrogel and ecoflex as the strain increases. Besides, upon extreme stretching, exceeding 700% strain, the SH-TENG can restore its original output performance without significant degradation when the external force is removed (Figure 4f).

2.4. Human Motion Detection Based on the SH-TENG. A part of the energy generated by the human body during exercise can be sensed by the flexible and stretchable hydrogel TENG sensors, and the mechanotransduction signals can be converted into visual electrical signals for feedback and display. It can be found that the TENG based on SA−Zn hydrogel has excellent electrical properties, which can instantly light up 234 commercial green LEDs by touching and pressing the SH-TENG with the contact area of 4 × 4 cm^2 (Figure 5a and Movie S3, Supporting Information). Here, the SH-TENG device is attached to the experimenter's wrist as shown in the inset in Figure 5b. When the experimenter's wrist is bent, the SH-TENG is stretched to contact with the skin, where the skin contacts with the silicone rubber to generate electrical signals, similar to the working mechanism of PMMA and silicone rubber mentioned earlier. The wrist keeps repeating the cycle of bending, and the output of the SH-TENG shows its good repeatability (Figure 5b). Based on its sensing property, it can also monitor the movements of the hands as a sensor. The bending amplitude of the SH-TENG was monitored by attaching it to a finger. The output of V_{OC} of the SH-TENG with various bending angles (from 30 and 60 to 90°) of the finger is illustrated in Figure 5c. The TENG sensing

https://doi.org/10.1021/acsami.1c12378
ACS Appl. Mater. Interfaces XXXX, XXX, XXX−XXX

mechanism of fingers and wrists in Figure 5b,c is the same as that in Figure 3c, just PMMA is converted to human skin. With increasing bending angle of the finger, the corresponding voltage output also increases linearly. The phenomenon is likely due to a greater contact pressure and smaller contact distance between the SH-TENG and the finger as the bending angle of the finger increases. In other words, the electrical output performance and the bending angle show a stable relationship.

In addition, the stretching motion of the human arm was tested by using a super stretchable SH-TENG smart training band system. In typical stretching for sports, the smart training band system should produce visual and readable signals, which can be used for human exercise arm strength monitoring, health monitoring, and equally important self-driven rehabilitation training. As we all know, with the development of the Internet of Things in the future, self-powered human health monitoring systems will attract wide attentions. The healthy people can acquire a series of parameters of their exercise based on the self-powered super-extendible TENG data, such as stretching force, exercise frequency, stretching times, and calories consumed during exercise. It is also possible to prepare different training plans according to different exercise requirements, such as increasing the number of stretch elastic bands and improving the stretching force or training intensity. The injured can use the force data of each stage of their dynamic exercises to formulate a rehabilitation training plan, regulating time, and stretching force. The working mechanism of the SH-TENG smart training band is illustrated in Figure S13.

Figure 5d shows that the hydrogel TENG is stretched by different forces and stretching lengths. On the basis of the above results, the monitoring of the arm stretching exercise under the super-stretchable hydrogel TENG was demonstrated. First, different output voltages were obtained under different tensions. According to this relationship, we simulate a linear graph (Figure 5e), that is, the formula

$$V_{OC} = 6.989F + 9.073 \quad (2)$$

where V_{OC} (V) is the voltage and F (N) is the force used for stretching. Here, the data are achieved using a single TENG elastic band, which can be stretched to a maximum distance of 150 cm (the experimenter's maximum exercise stretch can reach the data). The maximum distance requires a tensile force of 45 N, which can bring the voltage close to 350 V. We can increase the number of elastic bands to increase the tensile strength. On the contrary, when the voltage is known, the used tensile force can be obtained according to formula (2) in Figure 5e. At the same time, the consumed calories can be calculated by the exerciser based on the displacement of data during the stretching process. The final data are obtained according to the formula

$$\mathrm{Cal} = 4.186F \times L \quad (3)$$

where Cal (cal) is the calorie, L (m) is the movement displacement of stretching, and F (N) is the force used for stretching. According to the relationship between formulas (2) and (3), the linear relationship of calories and voltage can be finally achieved (Figure 5f), that is, the formula

$$\mathrm{Cal} = 0.044V_{OC} - 2.67 \quad (4)$$

Therefore, we can calculate the calorie data according to the output voltage obtained using the self-powered TENG based on formula (4). The finally obtained visual voltage signal can be collected and transformed through a specific transmission module. LabVIEW is a data processing software that can be programmed according to needs. It can analyze, judge, and calculate the received electrical signals synchronously according to the above formula. The visual interface and the real-time data of the stretching movement are obtained using software programming LabVIEW. The stretched numbers, real-time force, calories burned, and the data that can be customized according to customer needs can finally be presented on the software display interface. The real-time monitoring process of the smart arm training band sensor system during actual human motion is demonstrated in Figure 5h and Supplementary Movie S4,. The voltage output signal during exercise is shown in Figure 5g. It is found that when the SH-TENG works as an intelligent self-powered sensor, the mechanical energy of the human body can be converted into a real-time voltage signal by a signal acquisition and processing conversion system (Figure 5h). In addition, we can relevantly customize the system according to our requirements. For example, encouraging words appear in the pop-up window during exercising for a period of time. Besides, users can not only set the number of training sessions but also can pause and reset the interface of pop-up after achieving the requirements.

3. CONCLUSIONS

In summary, the ultrastretchable (>10,000%), highly transparent (>95%), and highly conducting (0.34 S m^{-1}) hydrogel electrolyte was used as an electrode to develop an SH-TENG, which was employed for energy harvesting for the fabrication of power sources and self-powered motion sensing. Furthermore, hydrogels with high elongation and conductivity can be used as ideal electrodes in other stretchable electronics. The SH-TENG was designed based on a simple structure of super-stretchable hydrogel encapsulated with elastic silicone rubber. The SA−Zn hydrogel endows the SH-TENG with super-stretchability, flexibility, and transparency. The optimal performance of the SH-TENG presents good linear response to tensile force, which shows gratifying performance in monitoring the stretching of the human body. It also can light up 234 green commercial LEDs easily. In addition, the SH-TENG self-powered elastic training band sensor based on conductive hydrogel was developed for monitoring data in stretching exercises. The proposed SH-TENG may have the potential applications in fields of medical monitoring and rehabilitation, electronic skins, self-powered sensors, and human−computer interaction in the future.

4. MATERIALS AND METHODS

4.1. Materials. Acrylamide (AM), acroleic acid (AA), SA, ammonium persulfate (APS), and $ZnSO_4{\cdot}7H_2O$, were supplied by Aladdin Chemical Co Ltd.

4.2. Fabrication of Stretchable SA−Zn Hydrogels. The hydrogels were synthesized by radical polymerization of SA, AA, and AM.[63] Primarily, 4.5 g of SA, 0.75 g of AA, 2.5 g of water, and 2.25 g of AM were all mixed together and stirring vigorously at room temperature until all monomers were completely dissolved, and then, the stirring was continued for 30 min. Then, 0.3 g of crushed $ZnSO_4{\cdot}7H_2O$ and untreated 4‰ (wt) APS were added to the above mixed solution in sequence and stirred vigorously at 1500 rpm for 60 min until there were no particles in the solution. If necessary, the stirring speed or stirring time was increased. Finally, the above reaction precursor solution was transferred to the PTFE mold (the size of the mold can be customized according to the size of the final required

https://doi.org/10.1021/acsami.1c12378
ACS Appl. Mater. Interfaces XXXX, XXX, XXX−XXX

hydrogel), sealed with plastic wrap, and reacted at 55 °C for 12 h to obtain an ultrastretchable SA−Zn hydrogel.

4.3. Preparation of the Flexible SH-TENG. The thickness of the hydrogel and SH-TENG are 1 and 2 mm, respectively. First, a elastomer ecoflex-0010 film (5 cm × 3 cm × 0.5 mm) was prepared with a mold. The elastomer ecoflex-0010 film was fabricated by mixing A and B base 1:1, followed by room temperature treatment for 4 h. Then, a 4 cm × 1 cm × 1 mm SA−Zn hydrogel was placed on the surface of ecoflex, and a Cu wire or an Al belt was attached to the hydrogel for electrical connection. Finally, a hollow rectangular mold (5 cm × 3 cm × 2 mm) was placed and fixed on the outer layer of the 5 cm × 3 cm × 0.5 mm elastomer ecoflex-0010 film, on which the hydrogel was placed. The elastomer ecoflex-0010 film liquid was cast to cover the hydrogel. After a while, the elastomer will solidify, that is, the casting thickness is 1.5 mm. The overall package thickness is 2 mm. After demolding, the SH-TENG is obtained by encapsulating the SA−Zn hydrogel with ecoflex films. The weight of the device is 0.98 g·cm^{-3}.The length and the thickness of the hydrogel inside the smart training band are 30 cm and 3 mm. The upper and lower thickness of the outer silicone rubber packaging layer is 4 mm. The total length of the whole elastic band is 32 cm.

4.4. Characterization and measurements. FTIR spectra were collected from samples in KBr pellets using a Nicolet 5700 FTIR instrument in a range of 400−4000 cm^{-1} at room temperature. The microtopography of SA−Zn hydrogel was tested using an FEI Quanta 250 filed emission scanning electron microscope. The stress−strain test of the SA−Zn hydrogel and TENG was performed using an ESM301/Mark-10 system. Unless otherwise specified, all stretching rates are fixed at 50 mm·min^{-1}. The UV−vis−NIR spectra for hydrogels were studied using a Shimadzu UV-3600 spectrophotometer at room temperature. Thermogravimetric analysis of the sample was carried out in a range of 25−650 °C and at a ramping rate of 10 °C·min^{-1} under argon atmosphere (TGA/DSC, Mettler Toledo). Real-time resistance was tested using a precision LCR meter (KEYSIGHT E4980AL). A linear motor (LinMot E1100) was used to provide the input of mechanical motions when driving the SH-TENG. The electric outputs were collected using a Keithley electrometer 6514.

■ ASSOCIATED CONTENT

Supporting Information

The Supporting Information is available free of charge at https://pubs.acs.org/doi/10.1021/acsami.1c12378.

Performance comparison of different contents of SA, APS, and $ZnSO_4·7H_2O$; FTIR, EIS, DSC, and TGA analysis of SA−Zn hydrogel; elastic modulus and stability analysis of SA−Zn hydrogel; different strain rates analysis and correlation between Young's modulus of SA−Zn hydrogel; working mechanism, V_{OC}, and power density of the SH-TENG under different strains; and electrical properties and stability analysis of SH-TENG (PDF)

Outstanding tensile stress-strain behavior of the SA−Zn hydrogel (MP4)

Conductivity of SA−Zn hydrogel (MP4)

Demonstration of lighting LEDs using SA−Zn hydrogel TENG (MP4)

Real-time response of the smart training band (MP4)

■ AUTHOR INFORMATION

Corresponding Authors

Kai Dong − *CAS Center for Excellence in Nanoscience Beijing Key Laboratory of Micro−Nano Energy and Sensor, Beijing Institute of Nanoenergy and Nanosystems, Chinese Academy of Sciences, Beijing 100083, P. R. China; School of Nanoscience and Technology, University of Chinese Academy of Sciences, Beijing 100049, P. R. China;* orcid.org/0000-0001-6314-1546; Email: dongkai@binn.cas.cn

Zhong Lin Wang − *CAS Center for Excellence in Nanoscience Beijing Key Laboratory of Micro−Nano Energy and Sensor, Beijing Institute of Nanoenergy and Nanosystems, Chinese Academy of Sciences, Beijing 100083, P. R. China; School of Nanoscience and Technology, University of Chinese Academy of Sciences, Beijing 100049, P. R. China; CUSTech Institute, Wenzhou, Zhejiang 325024, China; School of Material Science and Engineering, Georgia Inssstitute of Technology, Atlanta, Georgia 30332, United States;* orcid.org/0000-0002-5530-0380; Email: zhong.wang@mse.gatech.edu

Authors

Feifan Sheng − *School of Chemistry and Chemical Engineering, Center on Nanoenergy Research, School of Physical Science & Technology, Guangxi University, Nanning 530004, P. R. China; CAS Center for Excellence in Nanoscience Beijing Key Laboratory of Micro−Nano Energy and Sensor, Beijing Institute of Nanoenergy and Nanosystems, Chinese Academy of Sciences, Beijing 100083, P. R. China*

Jia Yi − *School of Chemistry and Chemical Engineering, Center on Nanoenergy Research, School of Physical Science & Technology, Guangxi University, Nanning 530004, P. R. China; CAS Center for Excellence in Nanoscience Beijing Key Laboratory of Micro−Nano Energy and Sensor, Beijing Institute of Nanoenergy and Nanosystems, Chinese Academy of Sciences, Beijing 100083, P. R. China*

Shen Shen − *CAS Center for Excellence in Nanoscience Beijing Key Laboratory of Micro−Nano Energy and Sensor, Beijing Institute of Nanoenergy and Nanosystems, Chinese Academy of Sciences, Beijing 100083, P. R. China*

Renwei Cheng − *CAS Center for Excellence in Nanoscience Beijing Key Laboratory of Micro−Nano Energy and Sensor, Beijing Institute of Nanoenergy and Nanosystems, Chinese Academy of Sciences, Beijing 100083, P. R. China; School of Nanoscience and Technology, University of Chinese Academy of Sciences, Beijing 100049, P. R. China*

Chuan Ning − *CAS Center for Excellence in Nanoscience Beijing Key Laboratory of Micro−Nano Energy and Sensor, Beijing Institute of Nanoenergy and Nanosystems, Chinese Academy of Sciences, Beijing 100083, P. R. China; School of Nanoscience and Technology, University of Chinese Academy of Sciences, Beijing 100049, P. R. China*

Liyun Ma − *CAS Center for Excellence in Nanoscience Beijing Key Laboratory of Micro−Nano Energy and Sensor, Beijing Institute of Nanoenergy and Nanosystems, Chinese Academy of Sciences, Beijing 100083, P. R. China*

Xiao Peng − *CAS Center for Excellence in Nanoscience Beijing Key Laboratory of Micro−Nano Energy and Sensor, Beijing Institute of Nanoenergy and Nanosystems, Chinese Academy of Sciences, Beijing 100083, P. R. China; School of Nanoscience and Technology, University of Chinese Academy of Sciences, Beijing 100049, P. R. China*

Wen Deng − *School of Chemistry and Chemical Engineering, Center on Nanoenergy Research, School of Physical Science & Technology, Guangxi University, Nanning 530004, P. R. China*

Complete contact information is available at: https://pubs.acs.org/10.1021/acsami.1c12378

Author Contributions

K.D. and Z.L.W. proposed and supervised the project. F.S. participated in all aspects of this work from device fabrication to characterization and data processing. J.Y. designed the structures of the SH-TENG. R.C. and C.N. were involved in device fabrication. L.M. and X.P. participated in capturing videos of equipment applications. S.S. and W.D. assisted in analyzing the data and co-writing the article. All authors discussed the results and commented on the article.

Notes

The authors declare no competing financial interest.

■ ACKNOWLEDGMENTS

The authors are grateful for the support received from the National Natural Science Foundation of China (grant no. 22109012), the Beijing Municipal Natural Science Foundation (grant no. 2212052), and the Fundamental Research Funds for the Central Universities (grant no. E1E46805). Informed consent was obtained from the volunteers who participated in the experiments.

■ REFERENCES

(1) Sun, Y.; Rogers, J. A. Inorganic Semiconductors for Flexible Electronics. *Adv. Mater.* **2007**, *19*, 1897−1916.
(2) Fan, F. R.; Tang, W.; Wang, Z. L. Flexible Nanogenerators for Energy Harvesting and Self-Powered Electronics. *Adv. Mater.* **2016**, *28*, 4283−4305.
(3) Pan, C.; Wu, H.; Wang, C.; Wang, B.; Zhang, L.; Cheng, Z.; Hu, P.; Pan, W.; Zhou, Z.; Yang, X.; Zhu, j. Nanowire-Based High-Performance "Micro Fuel Cells": One Nanowire, One Fuel Cell. *Adv. Mater.* **2008**, *20*, 1644−1648.
(4) Dong, K.; Peng, X.; Wang, Z. L. Fiber/Fabric-Based Piezoelectric and Triboelectric Nanogenerators for Flexible/Stretchable and Wearable Electronics and Artificial Intelligence. *Adv. Mater.* **2020**, *32*, 1902549.
(5) Dong, K.; Peng, X.; An, J.; Wang, A. C.; Luo, J.; Sun, B.; Wang, J.; Wang, Z. L. Shape Adaptable and Highly Resilient 3D Braided Triboelectric Nanogenerators as E-Textiles for Power and Sensing. *Nat. Commun.* **2020**, *11*, 2868.
(6) Xu, J.-L.; Liu, Y.-H.; Gao, X.; Shen, S.; Wang, S.-D. Toward Wearable Electronics: A Lightweight All-Solid-State Supercapacitor with Outstanding Transparency, Foldability and Breathability. *Energy Storage Mater* **2019**, *22*, 402−409.
(7) Zhang, Y.; Zhang, L.; Cui, K.; Ge, S.; Cheng, X.; Yan, M.; Yu, J.; Liu, H. Flexible Electronics Based on Micro/Nanostructured Paper. *Adv. Mater.* **2018**, *30*, 1801588.
(8) Yang, Y.; Gao, W. Wearable and Flexible Electronics for Continuous Molecular Monitoring. *Chem. Soc. Rev.* **2019**, *48*, 1465−1491.
(9) Kwon, Y. T.; Kim, Y. S.; Kwon, S.; Mahmood, M.; Lim, H. R.; Park, S. W.; Kang, S. O.; Choi, J. J.; Herbert, R.; Jang, Y. C.; Choa, Y. H.; Yeo, W. H. All-Printed Nanomembrane Wireless Bioelectronics Using A Biocompatible Solderable Graphene for Multimodal Human-Machine Interfaces. *Nat. Commun.* **2020**, *11*, 3450.
(10) Wu, H.; Huang, Y.; Xu, F.; Duan, Y.; Yin, Z. Energy Harvesters for Wearable and Stretchable Electronics: From Flexibility to Stretchability. *Adv. Mater.* **2016**, *28*, 9881−9919.
(11) Lee, J.; Llerena Zambrano, B.; Woo, J.; Yoon, K.; Lee, T. Recent Advances in 1D Stretchable Electrodes and Devices for Textile and Wearable Electronics: Materials, Fabrications, and Applications. *Adv. Mater.* **2020**, *32*, 1902532.
(12) He, X.; Zi, Y.; Guo, H.; Zheng, H.; Xi, Y.; Wu, C.; Wang, J.; Zhang, W.; Lu, C.; Wang, Z. L. A Highly Stretchable Fiber-Based Triboelectric Nanogenerator for Self-Powered Wearable Electronics. *Adv. Fun. Mater.* **2017**, *27*, 1604378.
(13) Xu, Z.; Wu, C.; Li, F.; Chen, W.; Guo, T.; Kim, T. W. Triboelectric Electronic-Skin Based on Graphene Quantum Dots for Application in Self-Powered, Smart, Artificial Fingers. *Nano Energy* **2018**, *49*, 274−282.
(14) Ma, L.; Wu, R.; Liu, S.; Patil, A.; Gong, H.; Yi, J.; Sheng, F.; Zhang, Y.; Wang, J.; Wang, J.; Guo, W.; Wang, Z. L. A Machine-Fabricated 3D Honeycomb-Structured Flame-Retardant Triboelectric Fabric for Fire Escape and Rescue. *Adv. Mater.* **2020**, *32*, 2003897−2003907.
(15) Paosangthong, W.; Torah, R.; Beeby, S. Recent Progress on Textile-Based Triboelectric Nanogenerators. *Nano Energy* **2019**, *55*, 401−423.
(16) Yin, R.; Wang, D.; Zhao, S.; Lou, Z.; Shen, G. Wearable Sensors-Enabled Human−Machine Interaction Systems: From Design to Application. *Adv. Fun. Mater.* **2021**, *31*, 2008936.
(17) Chen, X.; Xiong, J.; Parida, K.; Guo, M.; Wang, C.; Wang, C.; Li, X.; Shao, J.; Lee, P. S. Transparent and Stretchable Bimodal Triboelectric Nanogenerators with Hierarchical Micro-Nanostructures for Mechanical and Water Energy Harvesting. *Nano Energy* **2019**, *64*, 103904.
(18) Luo, J.; Tang, W.; Fan, F. R.; Liu, C.; Pang, Y.; Cao, G.; Wang, Z. L. Transparent and Flexible Self-Charging Power Film and Its Application in a Sliding Unlock System in Touchpad Technology. *ACS Nano* **2016**, *10*, 8078−8086.
(19) Song, W.; Yin, X.; Liu, D.; Ma, W.; Zhang, M.; Li, X.; Cheng, P.; Zhang, C.; Wang, J.; Wang, Z. L. A Highly Elastic Self-Charging Power System for Simultaneously Harvesting Solar and Mechanical Energy. *Nano Energy* **2019**, *65*, 103997.
(20) Fan, F.-R.; Tian, Z.-Q.; Lin Wang, Z. Flexible Triboelectric Generator. *Nano Energy* **2012**, *1*, 328−334.
(21) Lee, K. Y.; Chun, J.; Lee, J.-H.; Kim, K. N.; Kang, N.-R.; Kim, J.-Y.; Kim, M. H.; Shin, K.-S.; Gupta, M. K.; Baik, J. M.; Kim, S.-W. Hydrophobic Sponge Structure-Based Triboelectric Nanogenerator. *Adv. Mater.* **2014**, *26*, 5037−5042.
(22) Kwak, S. S.; Kim, S. M.; Ryu, H.; Kim, J.; Khan, U.; Yoon, H.-J.; Jeong, Y. H.; Kim, S.-W. Butylated Melamine Formaldehyde as A Durable and Highly Positive Friction Layer for Stable, High Output Triboelectric Nanogenerators. *Energy Environ. Sci.* **2019**, *12*, 3156−3163.
(23) Peng, X.; Dong, K.; Ye, C.; Jiang, Y.; Zhai, S.; Cheng, R.; Liu, D.; Gao, X.; Wang, J.; Wang, Z. L. A Breathable, Biodegradable, Antibacterial, and Self-Powered Electronic Skin Based on All-Nanofiber Triboelectric Nanogenerators. *Sci. Adv.* **2020**, *6*, No. eaba9624.
(24) Yi, J.; Dong, K.; Shen, S.; Jiang, Y.; Peng, X.; Ye, C.; Wang, Z. L. Fully Fabric-Based Triboelectric Nanogenerators as Self-Powered Human−Machine Interactive Keyboards. *Nano-Micro Let.* **2021**, *13*, 103.
(25) Ma, L.; Zhou, M.; Wu, R.; Patil, A.; Gong, H.; Zhu, S.; Wang, T.; Zhang, Y.; Shen, S.; Dong, K.; Yang, L.; Wang, J.; Guo, W.; Wang, Z. L. Continuous and Scalable Manufacture of Hybridized Nano-Micro Triboelectric Yarns for Energy Harvesting and Signal Sensing. *ACS Nano* **2020**, *14*, 4716−4726.
(26) Hinchet, R.; Yoon, H.-J.; Ryu, H.; Kim, M.-K.; Choi, E.-K.; Kim, D.-S.; Kim, S.-W. Transcutaneous Ultrasound Energy Harvesting Using Capacitive Triboelectric Technology. *Science* **2019**, *365*, 491−494.
(27) Zi, Y.; Niu, S.; Wang, J.; Wen, Z.; Tang, W.; Wang, Z. L. Standards and Figure-of-Merits for Quantifying the Performance of Triboelectric Nanogenerators. *Nat. Commun.* **2015**, *6*, 8376.
(28) Wang, Z. L. Triboelectric Nanogenerators as New Energy Technology and Self-Powered Sensors - Principles, Problems and Perspectives. *Faraday Discuss.* **2014**, *176*, 447−458.
(29) Dong, K.; Hu, Y.; Yang, J.; Kim, S.-W.; Hu, W.; Wang, Z. L. Smart Textile Triboelectric Nanogenerators: Current Status and Perspectives. *MRS Bull.* **2021**, *46*, 512−521.
(30) Kim, S.; Gupta, M. K.; Lee, K. Y.; Sohn, A.; Kim, T. Y.; Shin, K.-S.; Kim, D.; Kim, S. K.; Lee, K. H.; et al. Transparent Flexible

https://doi.org/10.1021/acsami.1c12378
ACS Appl. Mater. Interfaces XXXX, XXX, XXX−XXX

Graphene Triboelectric Nanogenerators. *Adv. Mater.* **2014**, *26*, 3918−3925.
(31) Zhang, P.; Guo, W.; Guo, Z. H.; Ma, Y.; Gao, L.; Cong, Z.; Zhao, X. J.; Qiao, L.; Pu, X.; Wang, Z. L. Dynamically Crosslinked Dry Ion-Conducting Elastomers for Soft Iontronics. *Adv. Mater.* **2021**, *33*, 2101396.
(32) Yi, F.; Wang, X.; Niu, S.; Li, S.; Yin, Y.; Dai, K.; Zhang, G.; Lin, L.; Wen, Z.; Guo, H.; Wang, J.; Yeh, M. H.; Zi, Y.; Liao, Q.; You, Z.; Zhang, Y.; Wang, Z. L. A Highly Shape-Adaptive, Stretchable Design Based on Conductive Liquid for Energy Harvesting and Self-Powered Biomechanical Monitoring. *Sci. Adv.* **2016**, *2*, 1501624−1501633.
(33) Yang, P.-K.; Lin, L.; Yi, F.; Li, X.; Pradel, K. C.; Zi, Y.; Wu, C.-I.; He, J.-H.; Zhang, Y.; Wang, Z. L. A Flexible, Stretchable and Shape-Adaptive Approach for Versatile Energy Conversion and Self-Powered Biomedical Monitoring. *Adv. Mater.* **2015**, *27*, 3817−3824.
(34) Wang, L.; Daoud, W. A. Highly Flexible and Transparent Polyionic-Skin Triboelectric Nanogenerator for Biomechanical Motion Harvesting. *Adv. Energy Mater.* **2019**, *9*, 1803183.
(35) Xiong, J.; Cui, P.; Chen, X.; Wang, J.; Parida, K.; Lin, M.-F.; Lee, P. S. Skin-Touch-Actuated Textile-Based Triboelectric Nanogenerator with Black Phosphorus for Durable Biomechanical Energy Harvesting. *Nat. Commun.* **2018**, *9*, 4280.
(36) Dinh Xuan, H.; Timothy, B.; Park, H. Y.; Lam, T. N.; Kim, D.; Go, Y.; Kim, J.; Lee, Y.; Ahn, S. I.; Jin, S. H.; Yoon, J. Super Stretchable and Durable Electroluminescent Devices Based on Double-Network Ionogels. *Adv. Mater.* **2021**, *33*, 2008849.
(37) Wang, J.; Wen, Z.; Zi, Y.; Zhou, P.; Lin, J.; Guo, H.; Xu, Y.; Wang, Z. L. All-Plastic-Materials Based Self-Charging Power System Composed of Triboelectric Nanogenerators and Supercapacitors. *Adv. Fun. Mater.* **2016**, *26*, 1070−1076.
(38) Jeong, Y. R.; Lee, G.; Park, H.; Ha, J. S. Stretchable, Skin-Attachable Electronics with Integrated Energy Storage Devices for Biosignal Monitoring. *Acc. Chem. Res.* **2018**, *52*, 91−99.
(39) Lu, C.; Chen, J.; Jiang, T.; Gu, G.; Tang, W.; Wang, Z. L. A Stretchable, Flexible Triboelectric Nanogenerator for Self-Powered Real-Time Motion Monitoring. *Adv. Mater. Technol.* **2018**, *3*, 1800021.
(40) Chen, M.; Zhang, L.; Duan, S.; Jing, S.; Jiang, H.; Li, C. Highly Stretchable Conductors Integrated with a Conductive Carbon Nanotube/Graphene Network and 3D Porous Poly(dimethylsiloxane). *Adv. Fun. Mater.* **2014**, *24*, 7548−7556.
(41) Mu, J.; Hou, C.; Wang, G.; Wang, X.; Zhang, Q.; Li, Y.; Wang, H.; Zhu, M. An Elastic Transparent Conductor Based on Hierarchically Wrinkled Reduced Graphene Oxide for Artificial Muscles and Sensors. *Adv. Mater.* **2016**, *28*, 9491−9497.
(42) Dickey, M. D. Stretchable and Soft Electronics using Liquid Metals. *Adv. Mater.* **2017**, *29*, 1606425.
(43) Yu, Z.; Zhang, Q.; Li, L.; Chen, Q.; Niu, X.; Liu, J.; Pei, Q. Highly Flexible Silver Nanowire Electrodes for Shape-Memory Polymer Light-Emitting Diodes. *Adv. Mater.* **2011**, *23*, 664−668.
(44) Hu, W.; Niu, X.; Li, L.; Yun, S.; Yu, Z.; Pei, Q. Intrinsically Stretchable Transparent Electrodes Based on Silver-Nanowire−Crosslinked-Polyacrylate Composites. *Nanotechnol* **2012**, *23*, 344022.
(45) Hyun, D. C.; Park, M.; Park, C.; Kim, B.; Xia, Y.; Hur, J. H.; Kim, J. M.; Park, J. J.; Jeong, U. Ordered Zigzag Stripes of Polymer Gel/Metal Nanoparticle Composites for Highly Stretchable Conductive Electrodes. *Adv. Mater.* **2011**, *23*, 2946−2950.
(46) Qi, J.; Wang, A. C.; Yang, W.; Zhang, M.; Hou, C.; Zhang, Q.; Li, Y.; Wang, H. Hydrogel-Based Hierarchically Wrinkled Stretchable Nanofibrous Membrane for High Performance Wearable Triboelectric Nanogenerator. *Nano Energy* **2020**, *67*, 104206.
(47) Wang, Y.; Zhang, L.; Lu, A. Highly Stretchable, Transparent Cellulose/PVA Composite Hydrogel for Multiple Sensing and Triboelectric Nanogenerators. *J. Mater. Chem. A* **2020**, *8*, 13935−13941.
(48) Yang, B.; Yuan, W. Highly Stretchable and Transparent Double-Network Hydrogel Ionic Conductors as Flexible Thermal-Mechanical Dual Sensors and Electroluminescent Devices. *ACS Appl. Mater. Interfaces* **2019**, *11*, 16765−16775.
(49) Sun, L.; Chen, S.; Guo, Y.; Song, J.; Zhang, L.; Xiao, L.; Guan, Q.; You, Z. Ionogel-Based, Highly Stretchable, Transparent, Durable Triboelectric Nanogenerators for Energy Harvesting and Motion Sensing Over A Wide Temperature Range. *Nano Energy* **2019**, *63*, 103847.
(50) Yuk, H.; Lu, B.; Zhao, X. Hydrogel Bioelectronics. *Chem. Soc. Rev.* **2019**, *48*, 1642−1667.
(51) Yang, C.; Suo, Z. Hydrogel Ionotronics. *Nat. Rev. Mater.* **2018**, *3*, 125−142.
(52) Wang, T.; Zhang, Y.; Liu, Q.; Cheng, W.; Wang, X.; Pan, L.; Xu, B.; Xu, H. A Self-Healable, Highly Stretchable, and Solution Processable Conductive Polymer Composite for Ultrasensitive Strain and Pressure Sensing. *Adv. Fun. Mater.* **2018**, *28*, 1705551.
(53) Guo, X.; Zhang, C.; Shi, L.; Zhang, Q.; Zhu, H. Highly Stretchable, Recyclable, Notch-Insensitive, and Conductive Polyacrylonitrile-Derived Organogel. *J. Mater. Chem. A* **2020**, *8*, 20346−20353.
(54) Zhou, Y.; Wan, C.; Yang, Y.; Yang, H.; Wang, S.; Dai, Z.; Ji, K.; Jiang, H.; Chen, X.; Long, Y. Highly Stretchable, Elastic, and Ionic Conductive Hydrogel for Artificial Soft Electronics. *Adv. Funct. Mater.* **2018**, *29*, 1806220.
(55) Shuai, L.; Guo, Z. H.; Zhang, P.; Wan, J.; Pu, X.; Wang, Z. L. Stretchable, Self-Healing, Conductive Hydrogel Fibers for Strain Sensing and Triboelectric Energy-Harvesting Smart Textiles. *Nano Energy* **2020**, *78*, 105389.
(56) Ganesh, R. S.; Yoon, H.-J.; Kim, S.-W. Recent Trends Of Biocompatible Triboelectric Nanogenerators Toward Self-Powered E-Skin. *EcoMat* **2020**, *2*, No. e12065.
(57) Zhang, P.; Chen, Y.; Guo, Z. H.; Guo, W.; Pu, X.; Wang, Z. L. Stretchable, Transparent, and Thermally Stable Triboelectric Nanogenerators Based on Solvent-Free Ion-Conducting Elastomer Electrodes. *Adv. Fun. Mater.* **2020**, *30*, 1909252.
(58) Huang, H.; Han, L.; Fu, X.; Wang, Y.; Yang, Z.; Pan, L.; Xu, M. Multiple Stimuli Responsive and Identifiable Zwitterionic Ionic Conductive Hydrogel for Bionic Electronic Skin. *Adv. Electron. Mater.* **2020**, *6*, 2000239.
(59) Han, L.; Huang, H.; Fu, X.; Li, J.; Yang, Z.; Liu, X.; Pan, L.; Xu, M. A Flexible, High-Voltage and Safe Zwitterionic Natural Polymer Hydrogel Electrolyte for High-Energy-Density Zinc-Ion Hybrid Supercapacitor. *Chem. Eng. J.* **2020**, *392*, 123733.
(60) Lai, J.-C.; Li, L.; Wang, D.-P.; Zhang, M.-H.; Mo, S.-R.; Wang, X.; Zeng, K.-Y.; Li, C.-H.; Jiang, Q.; You, X.-Z.; Zuo, J.-L. A Rigid and Healable Polymer Cross-Linked by Weak But Abundant Zn(II)-Carboxylate Interactions. *Nat. Commun.* **2018**, *9*, 2725.
(61) Wilson, E. W.; Hamilton, W. A.; Mount, H. R.; DeMore, W. B. Rate Constants for the Reactions of Hydroxyl Radical with Several Fluoroethers by the Relative Rate Method. *J. Phys. Chem. A* **2007**, *111*, 1610−1617.
(62) Jalababu, R.; Veni, S. S.; Reddy, K. V. N. S. Synthesis and characterization of dual responsive sodium alginate-g-acryloyl phenylalanine-poly N-isopropyl acrylamide smart hydrogels for the controlled release of anticancer drug. *J. Drug Delivery Sci. Technol.* **2018**, *44*, 190−204.
(63) Huang, H.; Han, L.; Li, J.; Fu, X.; Wang, Y.; Yang, Z.; Xu, X.; Pan, L.; Xu, M. Super-Stretchable, Elastic and Recoverable Ionic Conductive Hydrogel for Wireless Wearable, Stretchable Sensor. *J. Mater. Chem. A* **2020**, *8*, 10291−10300.

https://doi.org/10.1021/acsami.1c12378
ACS Appl. Mater. Interfaces XXXX, XXX, XXX−XXX